Thermal annealing induced structural, optical and electrical properties change in $As_{40}Se_{60-x}Bi_x$ chalcogenide thin films

Cite as: AIP Advances **9**, 095065 (2019); https://doi.org/10.1063/1.5111019
Submitted: 22 May 2019 • Accepted: 12 September 2019 • Published Online: 27 September 2019

Mukta Behera, N. C. Mishra, Ramakanta Naik, et al.

Thermal annealing induced structural, optical and electrical properties change in $As_{40}Se_{60-x}Bi_x$ chalcogenide thin films

Cite as: AIP Advances 9, 095065 (2019); doi: 10.1063/1.5111019
Submitted: 22 May 2019 • Accepted: 12 September 2019 •
Published Online: 27 September 2019

Mukta Behera,[1] N. C. Mishra,[1] Ramakanta Naik,[1,2,a)] C. Sripan,[3] and R. Ganesan[3]

AFFILIATIONS

[1]Department of Physics, Utkal University, Bhubaneswar 751004, India
[2]Institute of Chemical Technology-Indian Oil Odisha Campus, Bhubaneswar 751013, India
[3]Department of Physics, Indian Institute of Science, Bangalore 560012, India

[a)]Email: ramakanta.naik@gmail.com

ABSTRACT

This work reports the formation of topological Bi_2Se_3 phase upon annealing higher % of Bi content in amorphous $As_{40}Se_{60-x}Bi_x$ (x = 2, 7, 10 and 15%) chalcogenide thin films prepared by thermal evaporation process. The phase identification was done by X-ray diffraction study and Field emission scanning electron microscopy studies confirm the phase transformation in $As_{40}Se_{45}Bi_{15}$ thin film. The Raman measurements indicated the formation of crystalline As_4Se_4 and Bi_2Se_3 phase with annealing at 473K and the indirect optical band gap were found to decrease with increase in Bi concentration on thermal annealing as probed from the optical measurement. The changes in optical parameters were described on the basis of the density of localized states and the electrical resistance was found to be decreased which has been measured at room temperature by using the two-point probe technique.

I. INTRODUCTION

Due to the high transmission in infrared region of the light spectrum and photosensitive nature, chalcogenide materials have found themself for preparing infrared sensors, integrated optics and ultrahigh bandwidth signal processing.[1] Since, chalcogenide glasses occur in the non-equilibrium state due to sudden quenching, their different physical parameters must be relaxed which can be done by thermal annealing at different temperatures.[2] These parameters play a significant role in the optical properties of such materials in thin film form which have much importance from the device application point of view. Among them, phase transformation (amorphous-crystalline) due to external stimuli like laser irradiation, heat treatment, and ion irradiation is a significant one for rewritable optical memories and optical recording devices.[3–5] The simplest technique for tuning the optical parameters in chalcogenide thin films is done by thermal annealing which also brings changes in physical and chemical properties. Thermal annealing is a unique process for the phase transformation from amorphous to crystalline phase in glassy materials and such investigations give useful information regarding the mechanism of crystal growth and nucleation process.[6] It is a useful technique for the investigation of the reduction of intrinsic defects in amorphous state while transforming to crystalline phase which helps the chalcogenide materials for application in electrical switching and optical device.[7,8] The two types of new phase developed by thermal annealing in As_2Se_3 films brings a correlation between the two time scales measured through the refractive index.[9] The formation of $AgInSe_2$ phase from the Ag/In/Ag/In multilayer stack by thermal annealing is used for solar cell absorbing layer.[10] In a similar manner, the $AgIn_5Se_8$ phase was formed from the Ag/In_2Se_3 bilayer film upon thermal annealing at 250°C.[11] The amorphous-crystalline phase transformation in $Ge_{20}In_5Se_{75}$ thin film due to annealing changed the optical parameters to a great extent.[12] The annealing induced linear and nonlinear optical properties in $As_{47.5}Se_{47.5}Ag_5$ thin films are useful for optoelectronic applications.[13] The changes in optical parameters with annealing

temperature were described on the basis of structural relaxation as well as changes in defect states and density of localized states during amorphous to crystalline phase transformation in $Se_{85}In_{15-x}Zn_x$ thin films.[14] However, the annealing induced change in Bi doped films has shown strong thermoelectric power effect due the presence of Bi_2Se_3 phase.[15] The Bi_3Se_2 phase formation by thermal annealing of Bi/As_2Se_3 heterostructure film changed the optical, morphological and structural properties along with decrease in grain size.[16] The crystallized Se, In_2Se_3 and Bi_2Se_3 phases has been observed upon annealing the $Bi_xIn_{25-x}Se_{75}$ films at 440K which results decrease in band gap and change in electrical conductivity.[17] The annealing induced Bi diffusion into $GeSe_2$ layer at 250°C created Bi_2Se_3 phase that also decreased the optical band gap of the host material as explained on the basis of density of defect states and degree of disorder.[18] The annealing temperature affected the structure and optical properties of $Bi_5Ge_{40}Se_{55}$ thin films with evolution of two phases $GeSe_2$ and Bi_2Se_3.[19] So, crystallization of thermoelectric phase from the amorphous material could be a promising approach to get a thermoelectric material. The decrease in optical band gap (E_g) by annealing is an important feature specifically for optical recording memory.

In this regard, we have studied the effect of Bi addition into $As_{40}Se_{60}$ host matrix in our recent paper which shows amorphous nature of the films with change in optical properties.[20] However, in the present report we have shown the annealing effect on the structural, optical and electrical properties of $As_{40}Se_{60-x}Bi_x$ chalcogenide thin films that shows Bi_2Se_3 phase formation in 15% Bi content. The structural investigation is being done by X-ray diffraction (XRD) and Raman analysis. The optical property has been deduced from the transmission data in a wide spectral range of 500-1100nm. The surface morphology is being analysed from Field emission scanning electron microscopy (FESEM) and the elemental confirmation by Energy dispersive X-ray analysis (EDS).

II. EXPERIMENTAL TECHNIQUES

Bulk samples of $As_{40}Se_{60-x}Bi_x$ were prepared by melt quenching technique by taking highly pure (99.999%) As, Se and Bi (Sigma Aldrich). The constituent chemicals were weighed according to their atomic percentage and sealed in a chemically cleaned quartz ampoule with a vacuum of ~10^{-5} Torr. The sealed ampoule was kept inside a slow rotating furnace, and the temperature was raised with a heating rate 10 K/min up to 950°C and then kept constant for 24 h to make the melt homogeneous. After that, the ampoule was quenched in the ice-cooled water within a fraction of time to avoid the crystallization process.

The thin films of $As_{40}Se_{60-x}Bi_x$ were prepared by thermal evaporation process using a Hind High vacuum coating unit (HINDHIVAC Model 12A4D) on glass substrates kept at room temperature under the vacuum of ~5×10^{-5} Torr from the prepared bulk sample. The rate of deposition was fixed at 5nm/s, and the thickness of the film was ~800 nm which was controlled by using a quartz crystal monitor. To get the homogeneous and uniform film, the substrates were rotated slowly during the evaporation process. The temperature rise of the substrate due to radiant heating from crucible was negligible. The as-prepared films were annealed at 473 K for 2 hours inside the ceramic closed tubular furnace. After annealing, the samples were taken out after cooled down to room temperature.

The structural nature of annealed films was characterized by XRD (Bruker D8 advance) with copper target as a source of X-ray with λ = 1.54 *Å*. The scanning speed was maintained at 1°/min with a glancing angle of 2°. The morphological picture was taken by FESEM (ZEISS, SUPRA-40) set up in which EDS is attached that determined the elemental composition of the films. The optical transmittance measurements for the annealed $As_{40}Se_{60-x}Bi_x$ thin films have been carried out by using UV-Visible-NIR spectrophotometer (Bruker IFS 66v/s) over the 500–1200 nm wavelength range. The micro-Raman spectra of the studied films were recorded using a Raman Spectrometer (HORIBA T64000) with 514.5 nm Argon ion laser of power 1mW. The spectra were calibrated using the 520 cm^{-1} line of silicon thin film, and the spectra were taken with 40 seconds acquisition time. The I-V measurements were performed by using Agilent B2912A at room temperature in which Two – probe method was adopted.

III. RESULTS AND DISCUSSIONS

A. Structural analysis

Fig. 1 shows the XRD pattern of annealed $As_{40}Se_{60-x}Bi_x$ thin films that do not reveal any peak for x=2, 7 and 10% Bi content inferring the amorphous nature same as that of for the as-prepared film also.[20] However, the annealed film of 15% Bi composition shows XRD peaks at positions at 16.03°, 27.57° and 44.38°. The peak at 16.03° refers to As_4Se_4 phase (ICDD no. 71-0388) and 27.57°, 44.38° peaks refer to the Bi_2Se_3 phase (ICDD no. 77-2016). But, the as-prepared $As_{40}Se_{45}Bi_{15}$ film doesn't have any crystalline peak; however the bulk form is having the sharp peaks.[21] The segregation of Bi-rich clusters does not appear at smaller percentage of Bi due to its atoms are mixed homogeneously within the parent As-Se matrix. But at higher Bi % (15%), it enters into the As-Se network and its reaction with Se formed the Bi_2Se_3 crystalline phase. So the two different new phase formation in Bi

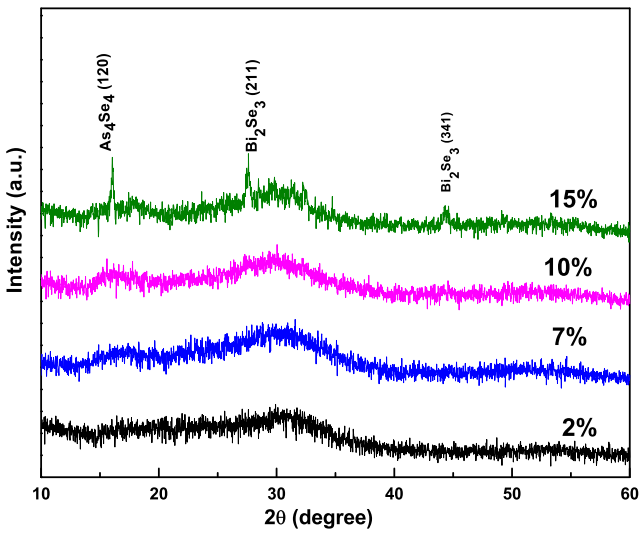

FIG. 1. XRD pattern of annealed $As_{40}Se_{60-x}Bi_x$ (x = 2, 7, 10 and 15%) thin films.

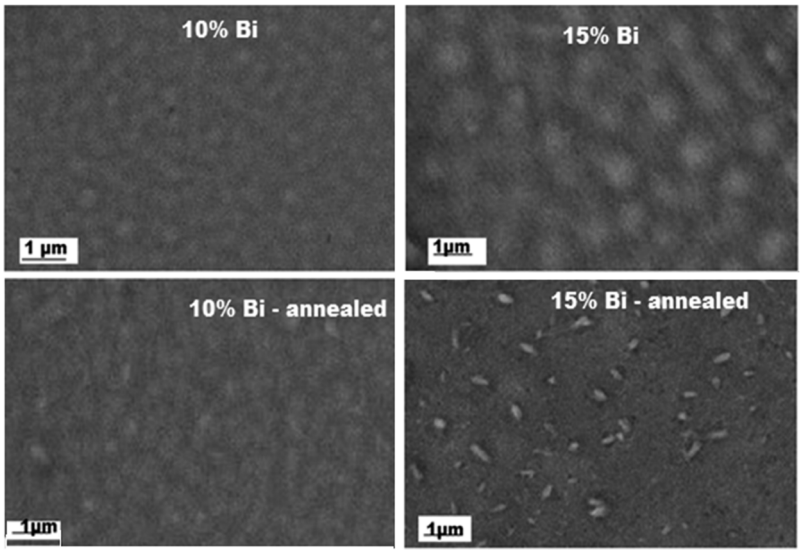

FIG. 2. FESEM images of as-prepared and thermally annealed $As_{40}Se_{60-x}Bi_x$ (x = 10 and 15%) thin films.

15% film shows the amorphous to crystalline transformation with annealing.

The crystallite size (D) of the two planes (211) and (341) corresponding to Bi_2Se_3 phase were determined using the well-known Sherrer X-ray diffraction formula[22]

$$D = \frac{0.9\lambda}{\beta\cos\theta} \quad (1)$$

where λ= 1.5406 Å is the Cu-Kα line wavelength, θ the Bragg diffraction angle and β the diffraction peak width (FWHM) expressed in radians. The estimated crystallite size was found to be 20.4 nm and 15 nm respectively.

The surface morphology as-prepared and annealed $As_{40}Se_{50}Bi_{10}$, $As_{40}Se_{45}Bi_{15}$ thin films are shown in Fig. 2. It is noticed that the microstructure of the 10% Bi film show a smooth and uniform surface after annealing at 200 °C which indicates the films are amorphous in nature. On the other hand in 15% Bi film after annealing a large no. of grains are formed during the crystallization process. This indicates the film consists of different rod-like shaped phases are embedded inside the glassy matrix.

The presence of the constituent elements before and after annealing for $As_{40}Se_{45}Bi_{15}$ film is presented by EDS spectra in Fig. 3. This also confirms the nearly stoichiometric composition after thermal annealing with slight variation. The calculated and observed concentration of the elements in Bi15% film is presented in Table I.

Fig. 4 shows the Raman spectra of annealed $As_{40}Se_{60-x}Bi_x$ (x = 2, 7, 10 and 15%) thin films in which we observed the Raman active peak (117 cm^{-1}) along with broadband centered at 228 cm^{-1}. This broad band has been attributed to As-Se vibration in $AsSe_3$ pyramidal units that is well agreed with that of the earlier reports.[23,24] The position of As-As vibrational mode along with the As-Se vibration doesn't change for the annealed film other than 15% Bi.

The annealed $As_{40}Se_{45}Bi_{15}$ film shows that the 117 cm^{-1} peak shifts towards higher wave number side (128 cm^{-1}) that corresponds to the vibrational mode of crystalline As_4Se_4 unit[25] and an extra peak is observed at 171 cm^{-1}. This peak corresponds to $A1g^2$ mode of Bi_2Se_3.[26] The Raman analysis revealed the evolution of two new crystalline As_4Se_4 and Bi_2Se_3 phases upon annealing,

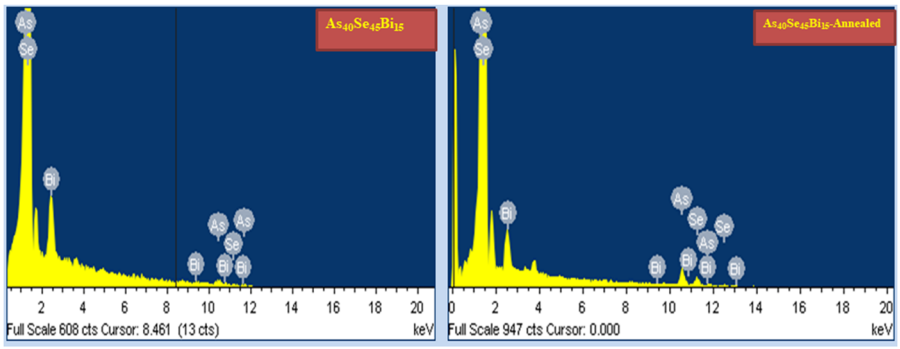

FIG. 3. EDS spectra of as-prepared and thermally annealed $As_{40}Se_{45}Bi_{15}$ film.

TABLE I. Elemental composition of as-prepared and annealed $As_{40}Se_{45}Bi_{15}$ thin films.

	15% Bi-as-prepared		15% Bi-annealed	
Element	Weight%	Atomic%	Weight%	Atomic%
As L	43.26	43.68	39.07	42.37
Se L	49.23	43.41	53.01	44.54
Bi M	07.51	12.91	07.92	13.09
Totals	100.00	100.00	100.00	100.00

which agrees with the XRD result of 15% Bi annealed films. The intensity of the 15% Bi film is more than that of the other films.

B. Optical analysis

UV-visible spectroscopy is an important technique for the optical characterization of materials. The transmission spectra of annealed $As_{40}Se_{60-x}Bi_x$ (x = 2, 7, 10 and 15 at %) films are presented in Fig. 5 in which transmission fringes arise nearly at 660 nm beyond the visible wavelength of light for the films except Bi 15%. The transmission percentage decreases and the absorption edge redshifts with increase in Bi concentration.[27,20] The absorption coefficient (α) was calculated from the transmission data with the help of thickness of the films by using the formula[28,29]

$$\alpha = \frac{1}{d} ln\left(\frac{1}{T}\right) \quad (2)$$

where d and T refers to the thickness and transmittance of the films respectively. The absorption coefficient is found to be increased with incident photon energy as well as with increase in Bi % as seen from Fig. 6.

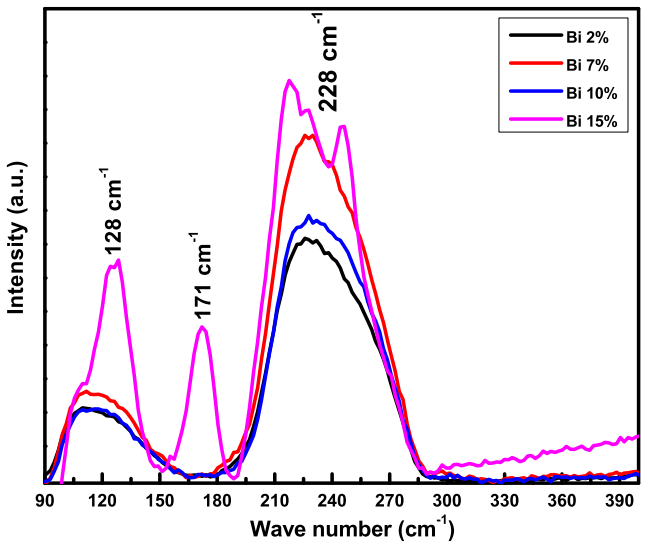

FIG. 4. Raman spectra of annealed $As_{40}Se_{60-x}Bi_x$ (x = 2, 7, 10 and 15%) thin films.

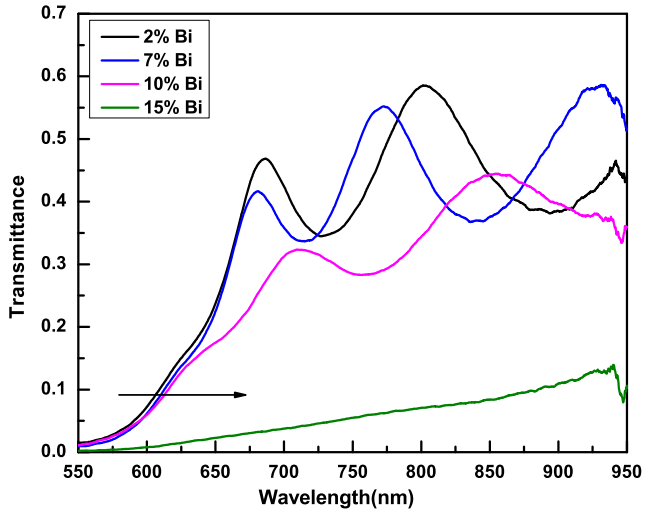

FIG. 5. Transmission spectra of thin films.

The increment of absorption coefficient with photon energy infers the higher absorption rate of incident radiation at higher frequency domain. The absorption coefficient due to the inter band transition is usually very large but it becomes very small when the photon energies fall below the energy band gap.

The absorption coefficient varies exponentially with photon energy at the lower values called as Urbach region that follows the relation

$$\alpha(h\nu) = \alpha_0 \exp\left(\frac{h\nu}{E_e}\right) \quad (3)$$

where ν, h and E_e are the frequency of the radiation, Planck's constant and Urbach energy respectively. The Urbach energy is expressed as the width of the localized states in the gap region and it generally presents the degree of disorder that characterizes the broadening of the absorption edge due to the electron-phonon

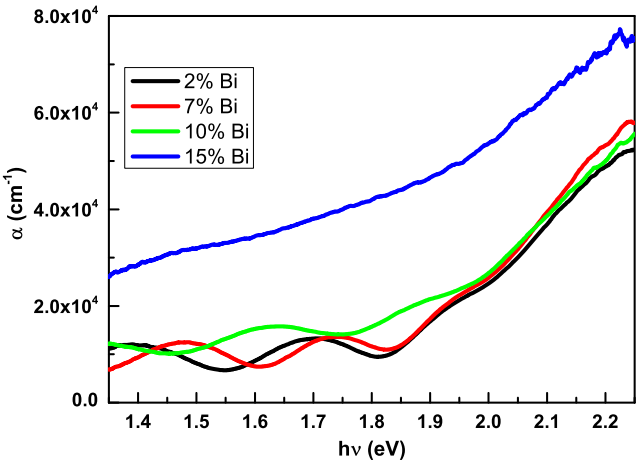

FIG. 6. Absorption coefficient spectra of thin films.

TABLE II. Optical and electrical parameters of $As_{40}Se_{60-x}Bi_x$ (2, 7, 10 and 15%) samples.

Samples	E_g (eV)	$B^{1/2}$ ($cm^{-1/2}eV^{-1/2}$)	Urbach energy (eV)	ρ(asp) (ohm.cm) $\times 10^6$	ρ(annl) (ohm.cm) $\times 10^5$
2% Bi	1.61±0.01	588±2	0.269	3.61	17.2
7% Bi	1.58±0.01	533±1	0.301	4.75	1.62
10% Bi	1.54±0.01	487±2	0.315	0.82	1.88
15% Bi	1.12±0.02	385±3	0.377	0.396	0.0427

interaction or excitation-phonon interaction in amorphous materials.[30] The mechanism of absorption process in this region usually depends on the transition probability between extended states and localized states of the two bands. So, the degree of disorder refers mostly on the electronic states within the material than the atomic arrangement. The calculated value of E_e as presented in Table II shows the increase in the width of the localized states in the gap region for which the optical band gap got reduced in our case like other studies also.[31,32]

But, in the high absorption edge region, the absorption coefficient obeys the relation[33]

$$\alpha h\nu = B(h\nu - E_g)^n \quad (4)$$

where B is a constant (Tauc parameter), E_g is the optical band gap, and n is an exponent which may take the values 2, 1/2, 2/3, and 1/3, depending on the absorption transition nature.[34] The best fit of the experimental results of the annealed thin films with n = 2 is shown in Fig. 7 that indicates the transition process is indirect allowed one. The variation of $(\alpha h\nu)^{1/2}$ with energy (hν) for the studied films is found to be identical to that of the elemental amorphous semiconductor.[35,36] The intercept of the straight line at the photon energy axis gives the optical band gap value as shown in Table I. The observed decrease in E_g value for the annealed films on increasing Bi % is well explained by Mott and Davis model which states the decrease in E_g is due to the increment in the density of localized states in such glassy system.[37] The defect states formed due to some dangling bonds are responsible for the creation of localized states. Many authors have shown that amorphous materials are transferred

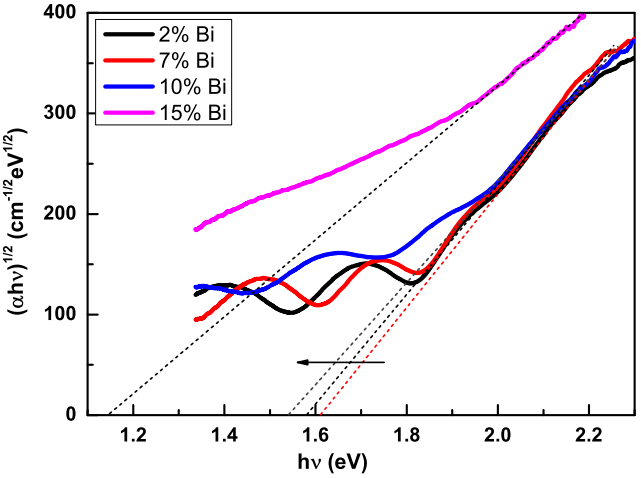

FIG. 7. $(\alpha h\nu)^{1/2}$ vs (hν) of annealed $As_{40}Se_{60-x}Bi_x$ (x = 2, 7, 10 and 15%) thin films.

to crystalline one under thermal annealing. So, during the process of crystallization some dangling bonds are produced. The formation of defects due to these dangling bonds causes tailing of bands into the band gap region. Again, thermal annealing breaks the larger crystallites into smaller crystals, thereby increasing the number of dangling bonds. So heat treatment of the films causes an increase

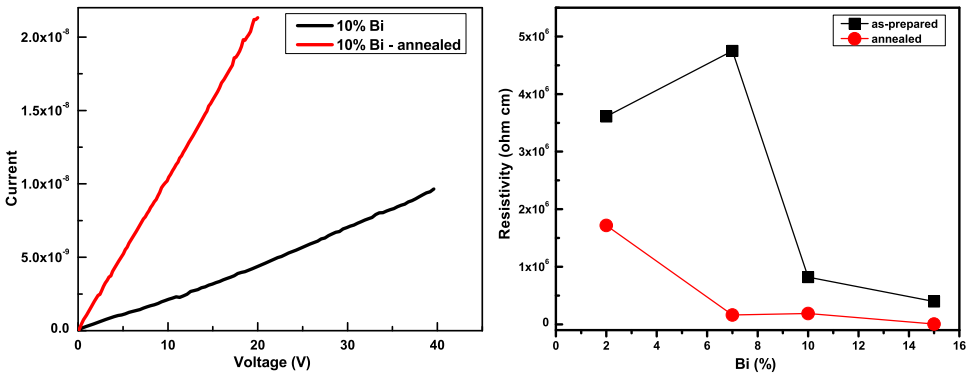

(a) (b)

FIG. 8. a. I-V plot for $As_{40}Se_{50}Bi_{10}$ thin film b. ρ variation in $As_{40}Se_{60-x}Bi_x$ thin films.

in the energy width of the localized states and hence reducing the optical energy gap. Annealing induced crystallization in 15% Bi film due to which band gap is reduced. The production of large number of surface dangling bonds around the crystallites forms some type of defect states in the gap region which leads to the reduction of optical gap.[38] So, the heterogeneous growth of crystalline phases and the increase in the metallic behavior augment the density of defect states associated with the surface of the crystallites to reduce the optical gap in these films. The variation in Tauc parameter as shown in Table I supports the optical change in the film due to the defect states.

C. Electrical properties

The performance of an electrical device depends on the resistivity of the material. The electrical resistivity of the films was measured by the D.C. two probe methods. I-V measurement of as-prepared and annealed $As_{40}Se_{60-x}Bi_x$ (2, 7, 10 and 15%) thin films are shown in Fig. 8. The linear I-V response was obtained for both as-prepared and annealed $As_{40}Se_{50}Bi_{10}$ thin films (Fig. 8a), which shows the current is proportional to the voltage applied according to Ohm's law. The variation of electrical resistivity with different Bi at% is shown in Fig. 8b which shows the decrease in resistivity with Bi %, hence the increase in electrical conductivity (Table II). The increase of conductivity is due to the shifting of Fermi level towards the middle of the band gap value.[39] The conductivity value is found to be increased more in case of annealed film as shown in Table II. Generally, the electrical conductivity of amorphous materials is lower than the crystalline materials. The improvement of crystallinity and decrease in gap between the two bands is responsible for the easy transport of charge carriers that increased the electrical conductivity.[40]

IV. CONCLUSION

The thermally evaporated thin films of $As_{40}Se_{60-x}Bi_x$ deposited on glass substrates were annealed out for the structural phase transformation and change in optical as well as electrical properties. The evolution of new topological phase Bi_2Se_3 was confirmed from the XRD and Raman study. The formation of crystallites in higher Bi % was seen from the FESEM picture. The indirect allowed optical band gap was found to be decreased due to the increase in width of localized states by defect states upon annealing. The increase in absorption coefficient with Bi concentration may be due to intrinsic absorption of more defect states in the boundaries and optical scattering. The decrease in electrical resistivity and increase in conductivity is due to the shifting of Fermi level towards the middle of the gap with the reduction of band gap.

ACKNOWLEDGMENTS

The authors thank IUAC, New Delhi for financial support (No. IUAC/XIII.7/UFR-58306) for JRF and Department of Physics, Indian Institute of Science (IISc.) for Optical and Raman measurement. The authors are also thankful to Dr. Kartik Senapati, NISER Bhubaneswar for helping in I-V measurement.

REFERENCES

[1] B. J. Eggleton, B. Luther Davis, and K. Richardson, Nat. Photonics **5**, 141 (2011).
[2] O. Nordman, N. Nordman, and N. Peyghambarian, J. Appl. Phys. **84**, 6055 (1998).
[3] H. Nyakotyo, T. S. Sathiaraj, and E. Muchuweni, Opt. Laser Technol. **92**, 182 (2017).
[4] A. T. Kawaguchi, A. V. Kolobov (Eds.), *Photo-Induced Metastability in Amorphous Semiconductors*, Wiley VCH, Weinheim, 2003, p. 182.
[5] B. A. Mansour, S. A. Gad, and H. M. Eissa, J. Non-Cryst. Solids **412**, 53 (2015).
[6] R. P. Tripathi, M. S. Akhtar, M. A. Alvi, and S. A. Khan, J. Mater. Sci. Mater. Electron. **27**, 8227 (2016).
[7] A. Zakery and S. R. Elliot, J. Non-Cryst. Solids **330**, 1 (2012).
[8] V. Takats, A. C. Miller, H. Jain, A. Kovalskiy, and S . Kokenyesi, Thin Solid Films **519**, 3437 (2011).
[9] R. P. Wang, S. J. Madden, C. J. Zha, A. V. Rode, and B. Luther-Davies, J. Appl. Phys. **100**, 063524 (2006).
[10] R. Panda, M. Panda, H. Rath, U. P. Singh, R. Naik, and N. C. Mishra, Opt. Mater. **84**, 618 (2018).
[11] R. Panda, R. Naik, and N. C. Mishra, J. Alloys Comp. **778**, 819 (2019).
[12] H. E. Atyia and N. A. Hegab, Optik **127**, 3888 (2016).
[13] E. R. Shaaban, M. Mohammed, M. N. Abd-el Saam, A. Y. Addel-Latief, M. A. Abdel-Rahim, and E. Sayed Yousuf, Opt. Mater. **86**, 318 (2018).
[14] A. Srivastava, S. N. Tiwari, M. A. Alvi, and S. A. Khan, J. Appl. Phys. **123**, 125105 (2018).
[15] J. Y. Hwang, H. A. Mun, and S. I. Kim, Inorg. Chem. **53**, 12732 (2014).
[16] M. Behera, N. C. Mishra, and R. Naik, Phys. B **560**, 51 (2019).
[17] S. Sharma, P. Kumar, and R. Thangaraj, Current Appl. Phys. **13**, 731 (2013).
[18] A. Aparimita, C. Sripan, R. Ganesan, and R. Naik, Opt. Mater. **89**, 157 (2019).
[19] F. M. Abdel-Rahim, M. M. Hafiz, and H. Alsorory, J. Alloys Comp. **570**, 76 (2013).
[20] M. Behera, R. Naik, N. C. Mishra, C. Sripan, and R. Ganesan, Current Appl. Phys. **19**, 884 (2019).
[21] M. Behera, R. Panda, N. C. Mishra, and R. Naik, Adv. Mat. Proc. **1**(2), 200 (2016).
[22] A. A. Al Ghamdi, S. A. Khan, A. Nagat, and M. S. Abd El-Sadek, Opt. Laser Technol. **42**, 1181 (2010).
[23] V. Kovanda, M. Vlcek, and H. Jain, J. Non-Cryst. Solids. **326**, 88 (2003).
[24] W. Li, S. Seal, C. Rivero, A. C. Miller *et al.*, J. Appl. Phys. **98**, 053503 (2005).
[25] N. Mateleshko, V. Mitsa, M. Veres, and M. Koos, J. Opt. Adv. Mat. **7**, 991 (2005).
[26] V. Gnezdilov, Yu. G. Pashkevich, H. Berger, E. Pomjakushina, K. Conder, and P. Lemmens, Phy. Rev. B **84**, 195118 (2011).
[27] M. M. Hafiz, A. A. Othman, M. M. El-Nahass, A. T. Al-Motasem, Physica B **390**, 348 (2007).
[28] K. Seedek, E. A. Mahamoud, F. S. Tera, A. Said, and S. M. El-Din, J. Phys. D: Appl. Phys. **27**, 156 (1994).
[29] R. Naik, C. Sripan, and R. Ganesan, Opt. Laser Techn. **90**, 158 (2017).
[30] J. D. Dow and D. Redfield, Phy. Rev. B **5**, 594 (1972).
[31] E. R. Shaaban, M. A. Kaid, E. S. Moustafa, and A. Adel, J. Phy. D: Appl. Phys. **41**, 125301 (2008).
[32] R. Naik, R. Ganesan, and K. S. Sangunni, Thin Solid Films **518**, 5437 (2010).
[33] J. Tauc, *The optical properties of solids* (North-Holland, Amsterdam, 1970).
[34] A. Aparimita, M. Behera, C. Sripan, R. Ganesan, S. Jena, and R. Naik, J. Alloys Comp. **739**, 997 (2018).
[35] A. Ahmad, S. A. Khan, L. Kumar *et al.*, Vacuum **82**, 608 (2008).
[36] P. Pradhan, P. Khan, J. R. Aswin, K. V. Adarsh, R. Naik, N. Das, and A. K. Panda, J. Appl. Phys. **125**, 015105 (2019).
[37] N. F. Mott and E. A. Davis, *Electronic Process in Non-Crystalline Materials* (Clarendon, Oxford, 1979).
[38] S. Chaudhuri and S. K. Biswas, J. Non-Cryst. Solids **54**, 179 (1983).
[39] A. El-Korashy, N. El-Kabany, and H. El-Zahed, Phys. B **365**, 55 (2005).
[40] X. Duan, J. Yang, W. Zhu, X. Fan, and C. Xiao, Mat. Lett. **61**, 4341 (2007).